

Dynamic calibration of the relative pose and error analysis in a structured light system

Beiwei Zhang^{1,2} and Youfou Li^{1,*}

¹Department of Manufacturing Engineering and Engineering Management, City University of Hong Kong, Hong Kong

²School of Information Engineering, Nanjing University of Financial and Economics, Nanjing, China

*Corresponding author: meyfli@cityu.edu.hk

Received July 2, 2007; revised November 24, 2007; accepted November 27, 2007;
posted January 2, 2008 (Doc. ID 84752); published February 11, 2008

We investigate the problem of dynamic calibration for our structured light system. First, a method is presented to estimate the rotation matrix and translation vector between the camera and the projector using plane-based homography. Then an approach is introduced to analyze theoretically the error sensitivity in the estimated pose parameters with respect to noise in the projection points. This algorithm is simple and easy to implement. Finally, some numerical simulations and real data experiments are carried out to validate our method.

© 2008 Optical Society of America

OCIS codes: 000.3110, 110.0110, 120.0120, 120.4640, 150.0150, 330.0330.

1. INTRODUCTION

In the past several decades, many approaches have been proposed to calibrate the intrinsic and extrinsic parameters of a vision system. These methods can be roughly classified into two categories: static calibration using a calibration object with known dimensions [1,2] and dynamic calibration that requires no reference target [3,4]. Dynamic calibration allows the system to recalibrate itself without any human intervention.

For some applications, we can concentrate on the extrinsic parameters, assuming that the intrinsic parameters are constant and calibrated offline. This is generally known as the relative pose problem in terms of the rotation matrix and translation vector. It is generally solved using one of the three approaches listed below:

(1) *Relative pose from the perspective- n -point problem* [5,6]. Starting from three or more corresponding point pairs, these methods attempt to determine the position and orientation of the camera with respect to a scene object. The major drawback is that some points from the scene should be provided as the control points. Hence, the methods cannot be applied to unknown scenes.

(2) *Using the fundamental matrix*. The fundamental matrix is a 3×3 matrix from which the extrinsic parameters can be recovered. It can be determined from eight or more corresponding point pairs using the eight-point algorithm [7,8]. Using singular value decomposition (SVD), Faugeras and Maybank [9] and Hartley [10] proposed a technique for factoring the fundamental matrix into a product of an orthogonal and a skew-symmetric matrix, which resulted in the solutions for the pose parameters. Recently, researchers have examined the possibility of determining the fundamental matrix using fewer than eight-correspondences, e.g., Triggs [11] and Nister [12]. The advantage of the eight-point algorithm is that it is linear and hence fast and easy to implement. However, it

will fail or give poor performance in the planar or near-planar environments since it requires a pair of images from the general 3D scene.

(3) *Using plane-based homography*. Hay [13] was the first to report his results in this domain. Tsai [14] and Longuet-Higgins [15] studied this problem using the SVD of plane-based homography. With eigenvalue decomposition of the homography matrix, as many as six cases were discussed according to different geometric situations in [16]. Using a model plane with known reference points, Ueshiba [17] gave a calibration algorithm for multicamera systems by factorizing the homography matrices. For the projector–screen–camera system, Rajj [18] and Okatani [19] investigated the calibration methods by treating the projectors as virtual cameras and using the principles of planar autocalibration. Recently, Habed and Boufama [20] formulated the self-calibration problem by solving the bivariate polynomial equations. Schweighofer and Pinz [21] suggested a robust approach for the pose estimation from a planar target by minimizing the object-space error. In [22], Mester and Muhlich presented an equilibrated total least-squares algorithm to improve motion and orientation estimation. In the presence of noise, uncertainty analysis of the calibration results is important for evaluating the performance of the vision system [23–26].

In practice, planar surfaces are encountered frequently in the surroundings either indoors or outdoors, e.g., desks, walls, or ground plane. So methods in the last category are highly desirable. However, the existing methods require either a complex mathematical manipulation or a nonlinear optimization process. In [27], we gave a simple and easy-to-implement algorithm for the relative pose problem by investigating the explicit formula of the homographic matrix. In this work, we provide an innovative closed-form solution for the pose parameters in order to increase the computational efficiency. Here an overcon-

straint system of equations is used to increase the robustness to noise. Finally, we determine the uncertainty in the estimated pose parameters using first-order perturbation theory. With this technique, we can predict the covariance matrix of the calibration results given noise in the image points.

The remainder of the paper is organized as follows: Section 2 gives a brief description of the structured light vision system. The schemes for determining the translation vector and rotation matrix and for analyzing their error sensitivity are presented in Sections 3 and 4, respectively. Section 5 reports some simulations and real data experimental results. In this paper, scales are denoted in italic letters, while vectors and matrices in boldface lowercase and uppercase letters, respectively. In addition, $\mathbf{0}_i$ and \mathbf{I}_i always represent the zero matrix and identity matrix, respectively, where the subscript “ i ” denotes the $i \times i$ matrix, and \otimes denotes the Kronecker product of two matrices.

2. SYSTEM DESCRIPTION

A. System Structure

Figure 1 depicts our vision system consisting of a projector and a camera. Here the projector, projecting a light pattern into the scene, is deemed as a virtual camera. The light pattern is distorted by the surface of the scene. These distortions are captured by the camera and used for calibration of the system and then reconstruction of the scene. For the camera and the projector, we define a right-handed coordinate system with its origin at their optical centers, respectively. Let the world coordinate system coincide with the camera coordinate system. Then the rotation matrix and translation vector from the camera to the projector, which are denoted by \mathbf{R} and \mathbf{t} , respectively, are the relative pose parameters in the system.

We assume that the intrinsic parameters for the camera and the projector have been calibrated, while their relative pose can be changed arbitrarily. We will focus on the following two problems: estimate (1) the relative pose between the camera and the projector and (2) the relationship between noise in the projection points and errors in the estimated pose parameters.

B. Computation of Plane-Based Homography

Given a 3D planar surface π in general position, its images in the camera and the projector are related by a

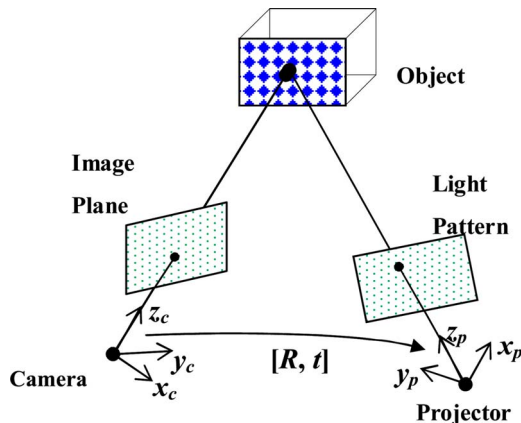


Fig. 1. (Color online) Relative pose of the proposed system.

3×3 homography matrix \mathbf{H} according to the projective geometry. Let \mathbf{M} be an arbitrary point on the plane and the correspondent projections be \mathbf{m}_c and \mathbf{m}_p , respectively. Then we have

$$\mathbf{m}_p = \sigma \mathbf{H} \mathbf{m}_c, \quad (1)$$

where σ is a nonzero scale factor. Let

$$\mathbf{H} = \begin{bmatrix} h_1 & h_2 & h_3 \\ h_4 & h_5 & h_6 \\ h_7 & h_8 & h_9 \end{bmatrix}$$

and its vector be

$$\mathbf{h} = (h_1, h_2, h_3, h_4, h_5, h_6, h_7, h_8, h_9)^T.$$

For the i th pair of projections, we denote $\mathbf{m}_c = [u_i \ v_i \ 1]^T$ and $\mathbf{m}_p = [u'_i \ v'_i \ 1]^T$.

According to Eq. (1), each pair of corresponding points provides two constraints on homography. So, given n ($n \geq 4$) pairs of corresponding image points of the scene, we have the following $2n$ equations:

$$\mathbf{A} \mathbf{h} = \mathbf{0}, \quad (2)$$

where:

$$\mathbf{A} = \begin{bmatrix} u_1 & v_1 & 1 & 0 & 0 & 0 & -u'_1 u_1 & -u'_1 v_1 & -u'_1 \\ 0 & 0 & 0 & u_1 & v_1 & 1 & -v'_1 u_1 & -v'_1 v_1 & -v'_1 \\ \vdots & \vdots \\ u_n & v_n & 1 & 0 & 0 & 0 & -u'_n u_n & -u'_n v_n & -u'_n \\ 0 & 0 & 0 & u_n & v_n & 1 & -v'_n u_n & -v'_n v_n & -v'_n \end{bmatrix}.$$

Let $\mathbf{Q} = \mathbf{A}^T \mathbf{A}$. Using eigenvalue decomposition, the solution for the vector \mathbf{h} can be determined by the eigenvector corresponding to the smallest eigenvalue of \mathbf{Q} .

C. Constraints from Homography

We assume that the equation of the plane π is $\mathbf{n}^T \mathbf{M} = 1$. For the calibrated camera and projector, the homography matrix can be expressed as

$$\mathbf{H} = \lambda (\mathbf{R} + \mathbf{t} \mathbf{n}^T), \quad (3)$$

where λ is a scale factor.

Let the translation vector be $\mathbf{t} = [t_1 \ t_2 \ t_3]^T$ and the skew symmetric matrix be

$$[\mathbf{t}]_x = \begin{bmatrix} 0 & -t_3 & t_2 \\ t_3 & 0 & -t_1 \\ -t_2 & t_1 & 0 \end{bmatrix}.$$

Multiplying matrix $[\mathbf{t}]_x$ to both sides of Eq. (3), we have

$$[\mathbf{t}]_x \mathbf{H} = \lambda [\mathbf{t}]_x \mathbf{R}. \quad (4)$$

As \mathbf{R} is a rotation matrix, $\mathbf{R} \mathbf{R}^T = \mathbf{I}$. By rearranging Eq. (4), we obtain

$$[\mathbf{t}]_x \mathbf{W} [\mathbf{t}]_x = \mathbf{0}, \quad (5)$$

where $\mathbf{W} = \mathbf{H} \mathbf{H}^T - \lambda^2 \mathbf{I}$ is a 3×3 matrix.

In the matrix \mathbf{W} , λ is unknown. In [27], we have proved that λ can be determined by the eigenvalue of matrix $\mathbf{H} \mathbf{H}^T$. There are always three eigenvalues for the matrix.

In that paper, we also gave a method to choose which one is correct. Once matrix \mathbf{W} is completely determined, the translation vector and rotation matrix can be calculated.

3. SOLVING THE RELATIVE POSE

A. Solution for the Translation Vector

As the translation vector is determined up to a nonzero scale factor, for simplicity, we assume that its third component is unity, i.e., $t_3=1$. There are six constraints on the translation vector in Eq. (5). By polynomial elimination of the quadratic items, we obtain the following three linear equations:

$$\begin{cases} a_1 t_1 + b_1 t_2 + c_1 = 0 \\ a_2 t_1 + b_2 t_2 + c_2 = 0 \\ a_3 t_1 + b_3 t_2 + c_3 = 0 \end{cases}, \quad (6)$$

where

$$a_1 = w_{13}w_{23} - w_{12}w_{33}, \quad b_1 = w_{11}w_{33} - w_{13}^2,$$

$$c_1 = w_{12}w_{13} - w_{11}w_{23},$$

$$a_2 = w_{22}w_{33} - w_{23}^2, \quad b_2 = w_{13}w_{23} - w_{12}w_{33},$$

$$c_2 = w_{12}w_{23} - w_{13}w_{22},$$

$$a_3 = w_{22}w_{13} - w_{12}w_{23}, \quad b_3 = w_{11}w_{23} - w_{12}w_{13},$$

$$c_3 = w_{12}^2 - w_{11}w_{22}.$$

Proposition 1: *The three linear equations in Eq. (6) are equivalent to one another.*

Proof. From Eq. (3), we have

$$\begin{aligned} \mathbf{H}\mathbf{H}^T &= \lambda^2 \mathbf{I} + \lambda^2 (\mathbf{R}\mathbf{n}\mathbf{t}^T + \mathbf{t}\mathbf{n}^T \mathbf{R}^T + \mathbf{n}^T \mathbf{n} \mathbf{t}\mathbf{t}^T) \\ &= \lambda^2 \mathbf{I} + \lambda^2 (\mathbf{s}\mathbf{t}^T + \mathbf{t}\mathbf{s}^T), \end{aligned} \quad (7)$$

where

$$\mathbf{s} = \mathbf{R}\mathbf{n} + \frac{\mathbf{n}^T \mathbf{n}}{2} \mathbf{t}.$$

Considering the definition of \mathbf{W} in Eq. (5), we obtain $\mathbf{W} = \lambda^2 (\mathbf{s}\mathbf{t}^T + \mathbf{t}\mathbf{s}^T)$.

In our system, we assume that the scene plane is opaque. Thus, in practice, the camera and the projector should lie on the same side of the plane and locate at different positions. Therefore, the two vectors \mathbf{t} and \mathbf{s} in Eq. (7) are nonzero and different from each other. Consequently, the rank of \mathbf{W} is 2 and the determinant of \mathbf{W} is zero, i.e.,

$$\begin{aligned} \det(\mathbf{W}) &= 2w_{12}w_{13}w_{23} - w_{23}^2w_{11} - w_{12}^2w_{33} - w_{13}^2w_{22} \\ &\quad + w_{11}w_{22}w_{33} = 0. \end{aligned}$$

From the first two equations in Eq. (6), we have

$$a_1 b_2 - a_2 b_1 = w_{33} \det(\mathbf{W}) = 0,$$

$$c_1 b_2 - c_2 b_1 = w_{13} \det(\mathbf{W}) = 0.$$

Therefore, they are equivalent to each other.

Similarly, the first and the third equations in Eq. (6) can be proved to be equivalent to each other. In summary, the three linear equations are equivalent to one another. \square

According to this proposition, we can use the first equation in Eq. (6) and another one in Eq. (5) to solve the translation vector. The solution can be described as follows:

$$\begin{cases} t_1 = \frac{w_{13} \pm \sqrt{w_{13}^2 - w_{11}w_{33}}}{w_{33}} \\ t_2 = \frac{(w_{13}w_{23} - w_{12}w_{33})t_1 + (w_{12}w_{13} - w_{11}w_{23})}{w_{11}w_{33} - w_{13}^2} \\ t_3 = 1 \end{cases}. \quad (8)$$

From Eq. (8), there are at most two solutions for the translation vector. In order to determine which one corresponds to the true configuration, the chirality constraint [28] can be employed.

B. Solution for the Rotation Matrix

By rearranging Eq. (4), we have

$$\mathbf{R}^T \mathbf{C} - \mathbf{D} = \mathbf{0}, \quad (9)$$

where $\mathbf{C} = \lambda[\mathbf{t}]_x$ and $\mathbf{D} = \mathbf{H}^T[\mathbf{t}]_x$.

We find that the above equation has the same form as that of Eq. (2.16) derived in [29]. Therefore, similar steps can be taken to solve the rotation matrix.

Assuming $\mathbf{C} = [\mathbf{C}_1 \ \mathbf{C}_2 \ \mathbf{C}_3]$ and $\mathbf{D} = [\mathbf{D}_1 \ \mathbf{D}_2 \ \mathbf{D}_3]$, we define a 4×4 matrix as

$$\mathbf{B} = \sum_{i=1}^3 \mathbf{B}_i^T \mathbf{B}_i, \quad (10)$$

where

$$\mathbf{B}_i = \begin{bmatrix} 0 & (\mathbf{C}_i - \mathbf{D}_i)^T \\ \mathbf{D}_i - \mathbf{C}_i & [\mathbf{C}_i + \mathbf{D}_i]_x \end{bmatrix}.$$

Let $\mathbf{q}_1 = (q_0 \ q_1 \ q_2 \ q_3)^T$ be the eigenvector of \mathbf{B} associated with the smallest eigenvalue. Then the solution for the rotation matrix \mathbf{R} is given as

$$\mathbf{R} = \begin{bmatrix} q_0^2 + q_1^2 - q_2^2 - q_3^2 & 2(q_1q_2 - q_0q_3) & 2(q_1q_3 + q_0q_2) \\ 2(q_1q_2 + q_0q_3) & q_0^2 - q_1^2 + q_2^2 - q_3^2 & 2(q_2q_3 - q_0q_1) \\ 2(q_1q_3 - q_0q_2) & 2(q_2q_3 + q_0q_1) & q_0^2 - q_1^2 - q_2^2 + q_3^2 \end{bmatrix}. \quad (11)$$

4. ERROR ANALYSES

Up to now, we have arrived at the solutions for the rotation matrix and translation vector. These solutions should be accurate in the absence of noise. However, noise is inevitable in the extracted feature points for a real application. It will affect the estimation of the homography matrix and consequently result in errors in the rotation matrix and translation vector. In the next three subsections, we will give a theoretical analysis on the corresponding error propagations.

A. Errors in the Homography Matrix

We first derive the error relationship between the homography matrix and the feature points according to Eq. (2).

In the structured light system, the projection point \mathbf{m}_p can be deemed as accurate since it is directly obtained from the predefined light pattern. Let the error vector in the i th image point \mathbf{m}_c be $\delta_{\mathbf{m}_c} = [\delta_{u_i}, \delta_{v_i}, 0]^T$. From Eq. (2), we can have the error matrix $\Delta_{\mathbf{A}}$ in matrix \mathbf{A} . Let $\delta_{\mathbf{A}^T}$ be the corresponding error vector of $\Delta_{\mathbf{A}}$ in the column first order. By first-order approximation, the error matrix $\Delta_{\mathbf{Q}}$ of matrix \mathbf{Q} can be computed by

$$\Delta_{\mathbf{Q}} = (\mathbf{A} + \Delta_{\mathbf{A}})^T(\mathbf{A} + \Delta_{\mathbf{A}}) - \mathbf{A}^T\mathbf{A} \approx \mathbf{A}^T\Delta_{\mathbf{A}} + \Delta_{\mathbf{A}}^T\mathbf{A}. \quad (12)$$

Rewriting the error matrix in column first order, we obtain

$$\delta_{\mathbf{Q}} = (\mathbf{F}_{\mathbf{Q}} + \mathbf{G}_{\mathbf{Q}})\delta_{\mathbf{A}^T}, \quad (13)$$

where

$$\mathbf{F}_{\mathbf{Q}} = \mathbf{A}^T \otimes \mathbf{I}_9, \quad \mathbf{G}_{\mathbf{Q}} = \begin{bmatrix} \mathbf{A}_1^1 & \mathbf{A}_1^2 & \cdots & \mathbf{A}_1^{2n} \\ \mathbf{A}_2^1 & \mathbf{A}_2^2 & \cdots & \mathbf{A}_2^{2n} \\ \cdots & \cdots & \cdots & \cdots \\ \mathbf{A}_9^1 & \mathbf{A}_9^2 & \cdots & \mathbf{A}_9^{2n} \end{bmatrix},$$

and \mathbf{A}_i^j denotes the matrix whose i th column is the j th row of \mathbf{A} , while other columns are all zero vectors.

Let \mathbf{v}_i and d_i be the i th eigenvector and eigenvalue of matrix \mathbf{Q} , respectively, and $\mathbf{V} = [\mathbf{v}_1 \ \mathbf{v}_2 \ \cdots \ \mathbf{v}_9]$. Applying the perturbation theory in [29] to Eq. (2), we have the first-order perturbation on the vector \mathbf{h}

$$\begin{aligned} \delta_{\mathbf{h}} &= \mathbf{V}\Lambda_{\mathbf{Q}}\mathbf{V}^T\Delta_{\mathbf{Q}}\mathbf{v}_1 = \mathbf{V}\Lambda_{\mathbf{Q}}\mathbf{V}^T[v_{11}\mathbf{I}_9 \ v_{21}\mathbf{I}_9 \ \cdots \ v_{91}\mathbf{I}_9]\delta_{\mathbf{Q}} \\ &= \mathbf{D}_{\mathbf{h}}\delta_{\mathbf{A}^T}, \end{aligned} \quad (14)$$

where $\Lambda_{\mathbf{Q}} = \text{diag}\{0, (d_1 - d_2)^{-1}, \dots, (d_1 - d_9)^{-1}\}$ and $\mathbf{D}_{\mathbf{h}} = \mathbf{V}\Lambda_{\mathbf{Q}}\mathbf{V}^T[v_{11}\mathbf{I}_9 \ v_{21}\mathbf{I}_9 \ \cdots \ v_{91}\mathbf{I}_9](\mathbf{F}_{\mathbf{Q}} + \mathbf{G}_{\mathbf{Q}})$. Equation (14) describes the error relationship between the image points and the homography matrix. With this relationship, the error δ_{λ^2} on λ^2 in Eq. (5) can be computed as follows.

Let $\mathbf{S} = \mathbf{H}\mathbf{H}^T$. Similar to Eqs. (12) and (13), we obtain the error vector for matrix \mathbf{S} as

$$\delta_{\mathbf{S}} = (\mathbf{F}_{\mathbf{S}} + \mathbf{G}_{\mathbf{S}})\delta_{\mathbf{h}} = \mathbf{D}_{\mathbf{S}}\delta_{\mathbf{h}}, \quad (15)$$

where

$$\mathbf{F}_{\mathbf{S}} = \mathbf{H}^T \otimes \mathbf{I}_3, \quad \mathbf{G}_{\mathbf{S}} = \begin{bmatrix} \mathbf{H}_1^1 & \mathbf{H}_1^2 & \mathbf{H}_1^3 \\ \mathbf{H}_2^1 & \mathbf{H}_2^2 & \mathbf{H}_2^3 \\ \mathbf{H}_3^1 & \mathbf{H}_3^2 & \mathbf{H}_3^3 \end{bmatrix}.$$

Let \mathbf{u}_2 be the eigenvector corresponding to the second eigenvalue of matrix \mathbf{S} . Using the perturbation theorem, the first-order perturbation on λ^2 is

$$\delta_{\lambda^2} = \mathbf{u}_2^T\Delta_{\mathbf{S}}\mathbf{u}_2 = \mathbf{u}_2^T[u_{12}\mathbf{I}_3 \ u_{22}\mathbf{I}_3 \ u_{32}\mathbf{I}_3]\delta_{\mathbf{S}}.$$

Then we have the relationship between δ_{λ^2} and $\delta_{\mathbf{A}^T}$,

$$\delta_{\lambda^2} = \mathbf{D}_{\lambda^2}\delta_{\mathbf{A}^T}, \quad (16)$$

where $\mathbf{D}_{\lambda^2} = \mathbf{u}_2^T[u_{12}\mathbf{I}_3 \ u_{22}\mathbf{I}_3 \ u_{32}\mathbf{I}_3]\mathbf{D}_{\mathbf{S}}\mathbf{D}_{\mathbf{h}}$. Assuming $|\delta_{\lambda^2}/\lambda^2| \ll 1$, the perturbation on λ is $\delta_{\lambda} = \sqrt{\lambda^2 + \delta_{\lambda^2}} - \lambda \approx \delta_{\lambda^2}/2\lambda$.

B. Errors in the Translation Vector

With Eqs. (15) and (16), we can obtain the error vector $\delta_{\mathbf{W}}$ for matrix \mathbf{W} in Eq. (5) as

$$\delta_{\mathbf{W}} = \delta_{\mathbf{S}} - [\mathbf{e}_1^T \ \mathbf{e}_2^T \ \mathbf{e}_3^T]^T\delta_{\lambda^2} = \mathbf{D}_{\mathbf{W}}\delta_{\mathbf{A}^T}, \quad (17)$$

where $\mathbf{D}_{\mathbf{W}} = \mathbf{D}_{\mathbf{S}}\mathbf{D}_{\mathbf{h}} - [\mathbf{e}_1^T \ \mathbf{e}_2^T \ \mathbf{e}_3^T]^T\mathbf{D}_{\lambda^2}$ and \mathbf{e}_i represents i th column of the identity matrix. Once we obtain the error for the matrix \mathbf{W} , the errors δ_{t_1} and δ_{t_2} for the translation vector can be computed as follows.

Expanding t_1 in Eq. (8) using a Taylor series for multiple variables, we have

$$\begin{aligned} t_1(w_{11}, w_{13}, w_{33}) &\approx t_1 - \frac{1}{2\sqrt{w_{13}^2 - w_{11}w_{33}}}\delta_{w_{11}} \\ &\quad + \left(\frac{1}{w_{33}} + \frac{w_{13}}{w_{33}\sqrt{w_{13}^2 - w_{11}w_{33}}} \right)\delta_{w_{13}} \\ &\quad + \left(\frac{w_{13}}{2w_{33}^2\sqrt{w_{13}^2 - w_{11}w_{33}}} - \frac{w_{13}}{w_{33}^2} \right)\delta_{w_{33}}. \end{aligned}$$

Similarly, we have the first-order approximation for t_2 . Expressing it in matrix form, we obtain

$$\begin{bmatrix} \delta_{t_1} \\ \delta_{t_2} \end{bmatrix} = [\mathbf{D}_{t_L} \ \mathbf{D}_{t_R}]\delta_{\mathbf{W}}, \quad (18)$$

where

$$\mathbf{D}_{t_L} = \frac{1}{b_1^2} \begin{bmatrix} -\frac{\sqrt{-b_1^3}}{2} & 0 & \frac{b_1^2 + w_{13}\sqrt{-b_1^3}}{w_{33}} \\ w_{23}b_1 + w_{33}b_1t_2 - \frac{a_1\sqrt{-b_1}}{2} & (w_{33}t_1 - w_{13})b_1 & \frac{w_{13}a_1\sqrt{-b_1} - a_1b_1}{w_{33}} - 2w_{13}b_1t_2 - (w_{23}t_1 + w_{12})b_1 \end{bmatrix},$$

and,

$$\mathbf{D}_{t_R} = \frac{1}{b_1^2} \begin{bmatrix} 0 & 0 & 0 & 0 & 0 & \frac{w_{11}\sqrt{-b_1^3 - 2w_{13}b_1^2}}{2w_{33}^2} \\ 0 & 0 & (w_{11} - w_{13}t_1)b_1 & 0 & 0 & w_{12}t_1b_1 + w_{11}t_2b_1 + \frac{w_{11}a_1\sqrt{-b_1} + 2w_{13}a_1b_1}{2w_{33}^2} \end{bmatrix},$$

where a_1 and b_1 are defined as in Eq. (6). Then the error relationship between the translation vector and the feature points can be described as

$$\delta_t = \mathbf{D}_t \delta_{A^T}, \quad (19)$$

where $\mathbf{D}_t = [\mathbf{D}_{t_L} \ \mathbf{D}_{t_R}] \mathbf{D}_W$.

C. Errors in the Rotation Matrix

To compute the errors in the rotation matrix, we first obtain the errors for matrix \mathbf{B} in Eq. (10).

For conciseness, we define a new vector \mathbf{p} that combines λ , t_1 , and t_2 with the vector \mathbf{h} such that $\mathbf{p} = [\lambda \ t_1 \ t_2 \ \mathbf{h}^T]^T$.

Considering Eqs. (14), (16), and (19), we have the error vector for \mathbf{p} as

$$\delta_p = \mathbf{D}_p \delta_{A^T}, \quad (20)$$

where $\mathbf{D}_p = [\mathbf{D}_{\lambda^2}/(2\lambda) \ \mathbf{D}_t \ \mathbf{D}_h]^T$.

Then the error vector for matrix \mathbf{B} can be expressed as

$$\delta_B = 2\mathbf{D}_B \delta_p, \quad (21)$$

where \mathbf{D}_B is given in Appendix A.

Let \mathbf{q}_i and γ_i be the i th eigenvector and eigenvalue of matrix \mathbf{B} , respectively, and $\boldsymbol{\eta} = [\mathbf{q}_1 \ \mathbf{q}_2 \ \mathbf{q}_3 \ \mathbf{q}_4]$. Using the perturbation theorem, the first-order perturbation on \mathbf{q}_1 is

$$\delta_{\mathbf{q}_1} = \boldsymbol{\eta} \boldsymbol{\Lambda}_B \boldsymbol{\eta}^T \Delta_B \mathbf{q}_1 = \mathbf{D}_{\mathbf{q}_1} \delta_p, \quad (22)$$

where q_i is the i th element of \mathbf{q}_1 , $\mathbf{D}_{\mathbf{q}_1} = 2\boldsymbol{\eta} \boldsymbol{\Lambda}_B \boldsymbol{\eta}^T [q_0 \mathbf{I}_4 \ q_1 \mathbf{I}_4 \ q_2 \mathbf{I}_4 \ q_3 \mathbf{I}_4] \mathbf{D}_B$, and $\boldsymbol{\Lambda}_B = \text{diag}\{0, (\gamma_1 - \gamma_2)^{-1}, (\gamma_1 - \gamma_3)^{-1}, (\gamma_1 - \gamma_4)^{-1}\}$.

In the column first order, the error on the rotation matrix can be computed as

$$\delta_R = \mathbf{J}_q \delta_q = \mathbf{D}_R \delta_{A^T}, \quad (23)$$

where \mathbf{J}_q represents the Jacobian matrix of the rotation matrix and $\mathbf{D}_R = \mathbf{J}_q \mathbf{D}_{\mathbf{q}_1} \mathbf{D}_p$.

In summary, the error vectors for the translation vector and rotation matrix can be expressed in terms of linear transformation of the errors of the coefficient matrix \mathbf{A} in Eq. (2). With Eqs. (19) and (23), their covariance matrices can be calculated as

$$\boldsymbol{\Gamma}_t = E(\delta_t \delta_t^T) = \mathbf{D}_t \boldsymbol{\Gamma}_{A^T} \mathbf{D}_t^T, \quad (24)$$

$$\boldsymbol{\Gamma}_R = E(\delta_R \delta_R^T) = \mathbf{D}_R \boldsymbol{\Gamma}_{A^T} \mathbf{D}_R^T, \quad (25)$$

where $E(\cdot)$ denotes the expectation.

We have analyzed the error relationships between the pose parameters and the image points. With these relationships, the accuracy of the calibration results can be predicted given the uncertainty of the image point localizations. Another potential use of the relationship is to provide a guideline for setting the system's configuration that can be expected to produce reasonable results.

5. EXPERIMENTAL RESULTS

A. Numerical Simulations

We have implemented a number of computer simulations on the proposed algorithms in MATLAB. The uncertainty in the pose estimates is determined for the following cases: varying number of correspondences for a fixed pose; varying amounts of noise for a fixed pose; and, finally, various poses. In each case, the relative errors for the translation vector \mathbf{t} and the three rotation angles $\boldsymbol{\xi} = [\alpha, \beta, \gamma]$ are respectively defined as $\|\mathbf{t} - \bar{\mathbf{t}}\|/\|\mathbf{t}\|$ and $\|\boldsymbol{\xi} - \bar{\boldsymbol{\xi}}\|/\|\boldsymbol{\xi}\|$, where $\bar{\mathbf{t}}$ and $\bar{\boldsymbol{\xi}}$ were the estimated values. We assumed that a virtual planar target was projected to the projector plane and camera image. The image resolution

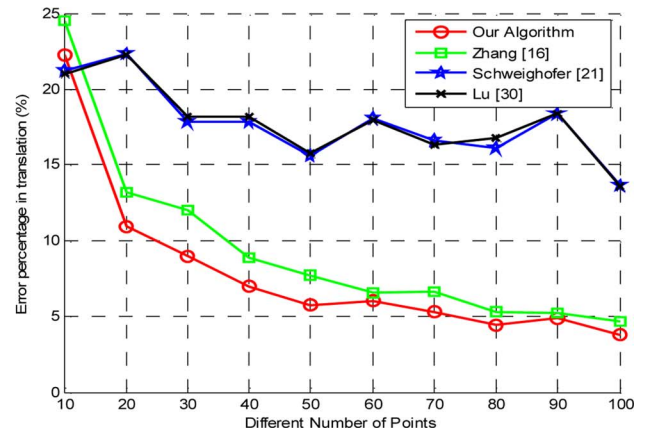
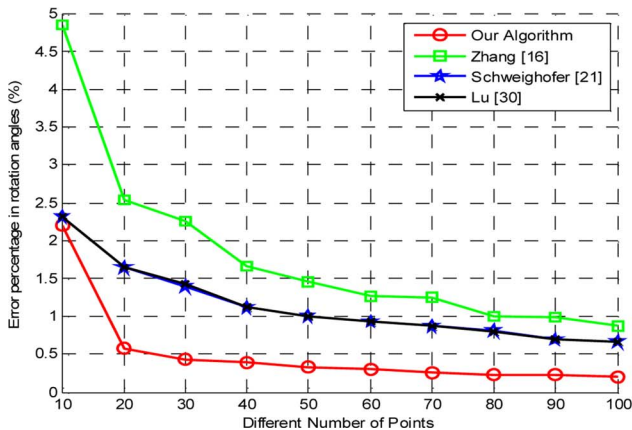


Fig. 2. (Color online) Relative errors for the rotation and translation versus number of points for the pose estimation.

Table 1. Comparison of the Computational Efficiency

No. of Points	Time Elapsed in the Simulations (s)			
	Our Algorithm	Algorithm of [16]	Algorithm of [30]	Algorithm of [21]
10	0.0045	0.0016	0.2686	0.2612
30	0.0041	0.0020	0.2659	0.2961
50	0.0053	0.0031	0.3544	0.3604
70	0.0053	0.0027	0.4352	0.4242
90	0.0044	0.0036	0.5250	0.4774
100	0.0056	0.0027	0.5623	0.5080

is 740×480 . The projection points were corrupted by random Gaussian noise with various deviations and zero mean, and the average results over 100 trials were reported. In these simulations, we made comparisons to the following three algorithms:

- An algorithm very similar to ours in Zhang [16], which solves the relative pose problem by decomposition of the planar homography. In all the graphs, we used red circle (○) and green square (□) to indicate our algorithm and Zhang’s, respectively.
- Robust pose estimation algorithms with iterative optimization in [21,30]. (Here the algorithms are randomly

initialized since they are globally convergent.). We signified them by a blue star (☆) and black cross (×).

Dependence on the number of points: In the first simulation, we studied the dependence of these algorithms on different numbers of point correspondences. Here the number of points ranged from 10 to 100, and random noise with 0.5 pixel variance was added to the image points. Figure 2 shows that improved performance was obtained when more points were used. However, when the number is larger than 50, the improvement is trivial. In this simulation, the elapsed time was recorded as in Table 1. From this table, we can see that the time roughly increased, since more computations are required with more points. As our algorithm and Zhang’s provide closed-form solutions, they are computationally more efficient than the other two algorithms.

Dependence on the noise level: In this simulation, we varied the level of Gaussian noise from 0 to 1.0 pixel and reported the relative errors of the four algorithms in Fig. 3. It is observed that the relative errors increase with increased noise level. The iterative algorithms are more robust in the estimation of the rotation matrix than in that of the translation vector, while the opposite is true for Zhang’s. On the whole, our algorithm outperforms the others in the presence of noise.

Dependence on the random pose: Figure 4 illustrates the performance of these algorithms in ten randomly se-

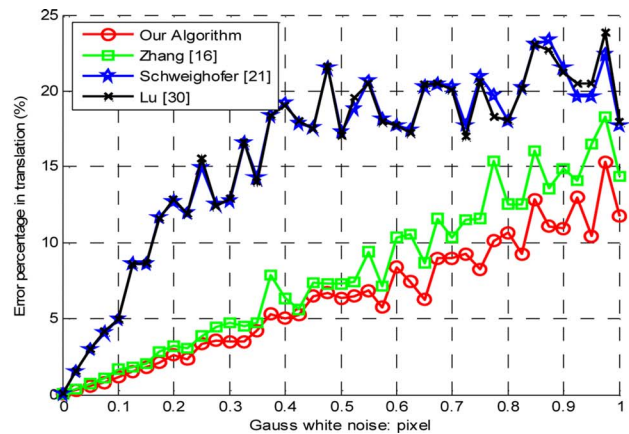
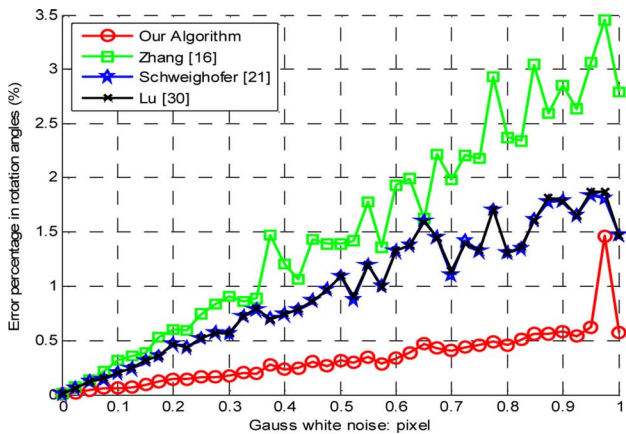


Fig. 3. (Color online) Relative errors for the rotation and translation as a function of injected noise.

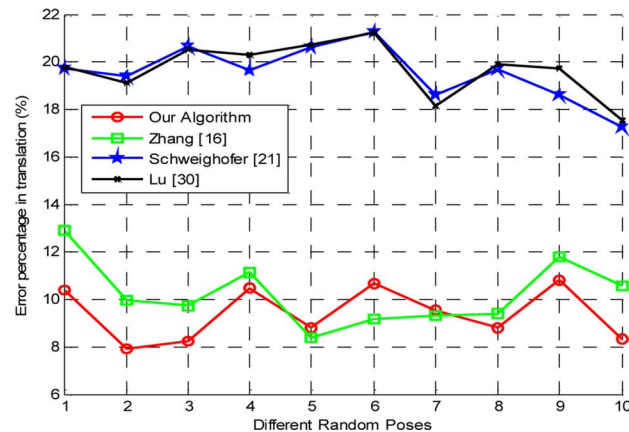
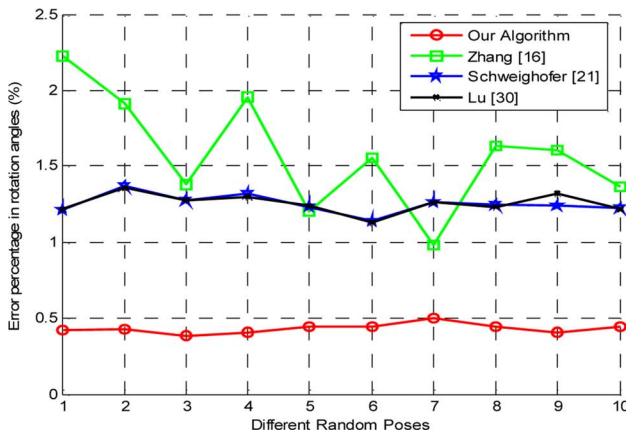


Fig. 4. (Color online) Relative errors for the rotation and translation as a function of different random poses.

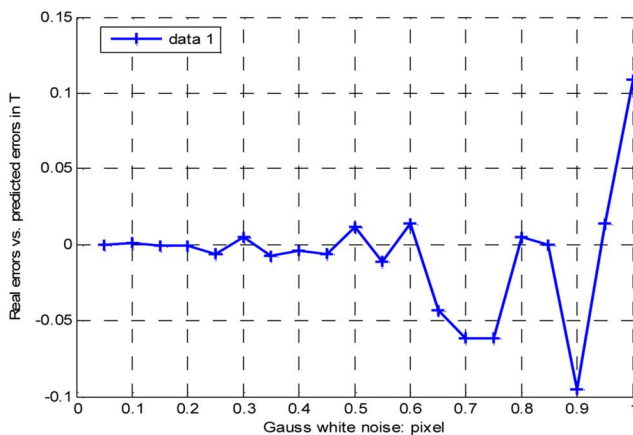
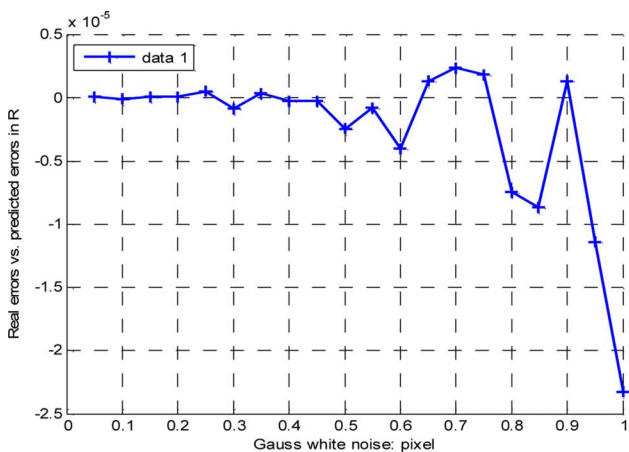


Fig. 5. (Color online) Test on the accuracy of the error prediction method, where data1 denotes the difference between real errors and predicted errors.

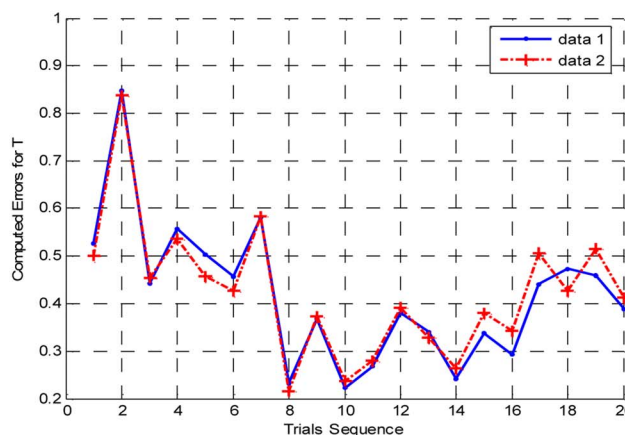
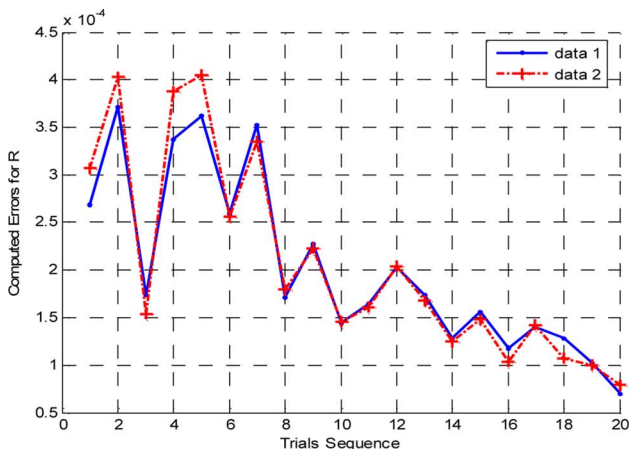
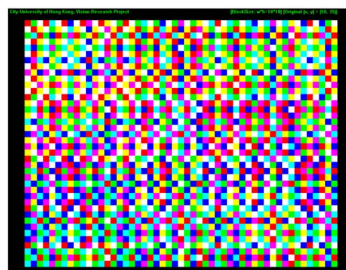


Fig. 6. (Color online) Test on different pose parameters, where data1 and data2 represent the computed errors and the predicted errors, respectively.



(a)



(b)

Fig. 7. (Color online) Configuration of our structured light system: (a) experimental setup and (b) screen shot of the color-encoded light pattern.

lected relative poses. Gaussian noise with a 0.5 pixel variance was added to the projection points, and 100 trials were run for each pose. It is observed that Zhang’s algorithm is very sensitive to the estimation of the rotation matrix, while the iterative algorithms are sensitive to that of the translation vector. Our algorithm gives considerably stable performance for all the poses.

Test on the error prediction algorithm: To evaluate the accuracy of our error prediction method, we compared the predicted errors and the computed errors in the simulations. The differences between the rotation matrix and the translation vector are given in Fig. 5. From these fig-

ures, we can see that the differences are very small, especially when the level of noise is low, say, below 0.5 pixels. As a result, the predicted errors are very close to the real ones. This demonstrates that the error analysis is valid.

In the last simulation, we carried out some experiments on the computed errors and the predicted errors for different pose parameters. Since the rotation parameters did not significantly affect the solutions, we just tested for different translation vectors. Here the direction of the translation vector was changed from [3,0,1] to [0,8,1] with 20 evenly distributed directions. Random noise with a 0.5 pixel variance was added to the projection points. For

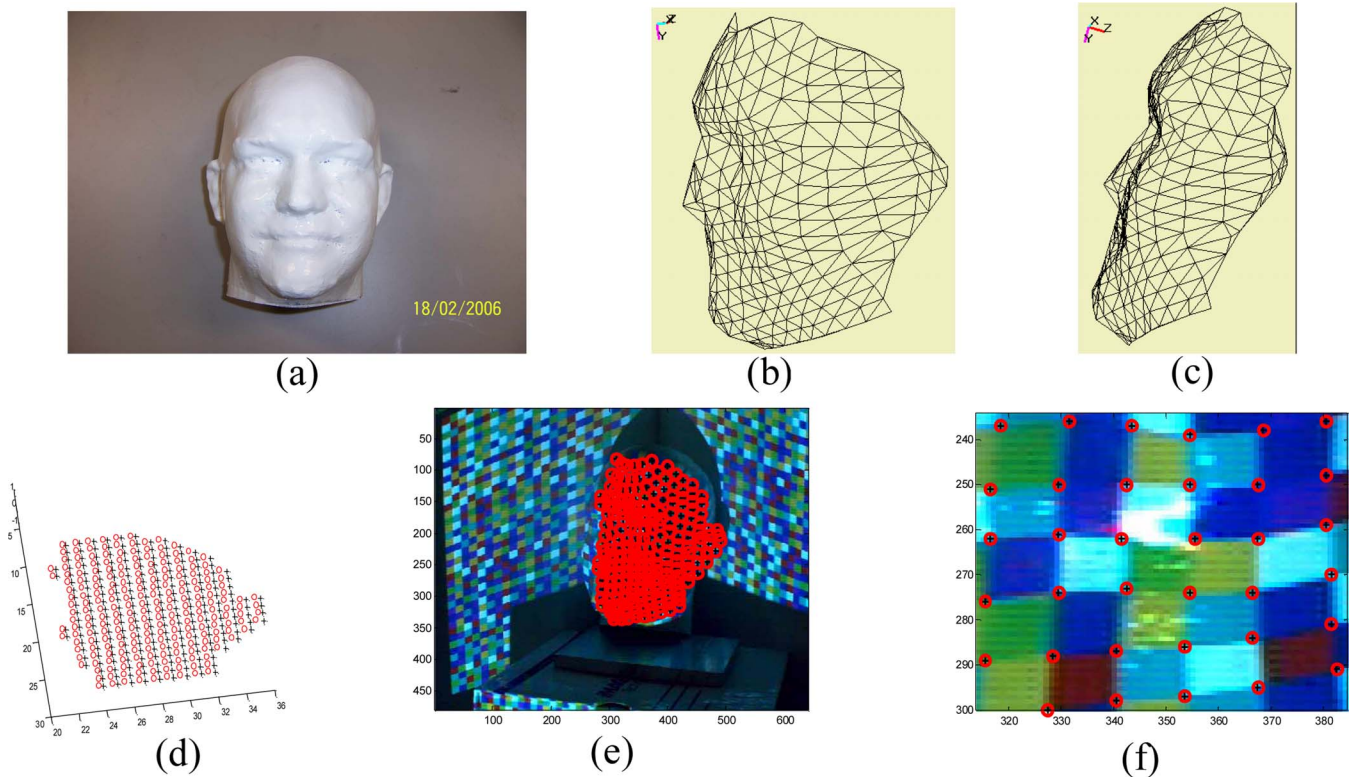


Fig. 8. (Color online) Experiment on the man's head model: (a) man's head model used for the experiment; (b, c) polygonized results of the points clouds in two different viewpoints; (d, e, f) original feature points and reprojected points, where blue “+” represents original feature points while red “o” represents reprojected points from reconstructed 3D points. They should coincide with each other theoretically.

each direction, ten trials were performed, and the average results for the rotation matrix and translation vector are shown in Fig. 6. As can be seen from this figure, the predicted errors are strongly correlated with the computed errors. The first several trials are more sensitive to noise and hence more unreliable; e.g., the errors for both the rotation matrix and the translation vector in the second trial are larger than the rest.

In these simulations, we find that the translation is more sensitive to noise compared to rotation. Theoretically, these results are due to the different weight matrices in Eqs. (24) and (25), i.e., D_t and D_R . In these experiments, we find that the matrix D_t has a larger effect on the translation vector than D_R has on the rotation matrix.

B. Real Data Experiments

Figure 7(a) shows the system setup for real data experiments, which consists of a PULNIX TMC-9700 CCD camera and a PLUS V131 DLP projector. Figure 7(b) gives the color-encoded light pattern for the projector used to uniquely identify the correspondences between the projector plane and the image plane [31].

The intrinsic parameters of the camera and the projector were first calibrated by a planar pattern using Zhang's method [32]. In the experiments, we placed the pattern at

Table 2. Relative Pose of the Vision System

Rotation angles	$[-2.1691, 2.1397, 0.3903]$
Translation vector	$[50.1919, -28.8095, 1]$

more than two different positions to increase the calibration accuracy. When calibrating the extrinsic parameters, more than four point correspondences from a planar surface in the scene were chosen between the projector plane and the camera image. The computed homography matrix was $h = [-0.4047, 1.0547, -0.3501, 1.2877, 0.0416, 0.0373, 0.2386, -0.1385, 1.0356]$. Then, using our method, the results for the three rotation angles and translation vector were obtained and are given in Table 2.

After the system had been calibrated, 3D object reconstruction was performed to test the calibration results. Figure 8(a) gives an image of a man's head model. In total, 226 points from the model were reconstructed. Here the polygonized results of the reconstructed point clouds were shown from two different viewpoints as in Figs. 8(b) and 8(c). Since no ground truth was available, we did not know the real values of the pose parameters of the system and the 3D point clouds. To test the accuracy of the experimental results, we measured the absolute errors between backprojected images of the reconstructed 3D

Table 3. Comparison of the Mean Absolute Errors

Different Methods	Camera (pixel)	Projector (pixel)
Fofi's results		
Linear algorithm	18.428	32.751
Iterative algorithm	0.204	0.169
Our results		
Linear algorithm	0.0217	0.2906

points and the real image features. In general, the more accurate the calibrated pose parameters, the smaller the errors. Figures 8(d) and 8(e) show the feature points and backprojected points for the projector plane and the camera image, respectively. Figure 8(f) shows a zoomed part of the image. It is seen that the original feature points and the backprojected points are very close to each other. Here we also give a numerical evaluation on the absolute errors in pixel dimensions in Table 3. For comparison, we listed the mean results together with those of the first real data experiment from Fofi *et al.* [33]. In that work, a completely different algorithm was proposed using the fundamental matrix on a similar vision system. Considering that only a linear algorithm is involved in our method, our results show a nontrivial improvement over Fofi's. So this experiment validates our algorithm both qualitatively and quantitatively.

6. CONCLUSIONS

We have presented our work on the relative pose problem in a structured light system. The contributions can be summarized into the following three aspects:

First, a closed-form solution for the pose parameters is provided by using plane-based homography. Our method is computationally efficient, since time-consuming nonlinear optimization is avoided. Furthermore, overdetermined constraints are established to enhance the robust-

ness; e.g., six equations are constructed to solve two variables in the translation vector. Second, based on matrix perturbation theory, error analysis and propagation for the estimated pose parameters are derived. These errors provide a possible means for studying the robustness of the solutions and a guideline for setting the system's configuration in practical applications. Last, numerical simulations and real data experiments are performed on the proposed system. The results are evaluated qualitatively and quantitatively and compared with existing algorithms. There are also some limitations with this method. The proposed normalization for estimating the translation vector is not suited for dominant sideways motion.

Our assumption of a planar surface can be satisfied in many practical situations. In fact, planar or near-planar scenes are encountered frequently, e.g., roadways or ground planes in mobile robot navigation and walls or ceilings for a climbing robot. In many practical applications where the traditional methods may fail or give a poor performance, since they require a pair of images from the 3D scene, our method provides a good solution.

APPENDIX A

We assume that c_{ij} and d_{ij} are the (i,j) elements of matrix \mathbf{C} and \mathbf{D} in Eq. (9), respectively.

Let $\mathbf{D}_B = [\mathbf{D}_\lambda \mathbf{D}_{t_1} \mathbf{D}_{t_2} \mathbf{D}_{h_L} \mathbf{D}_{h_R}]$. From Eq. (21), the five elements in \mathbf{D}_B can be expressed as follows:

$$\mathbf{D}_\lambda = \begin{bmatrix} d_{31}t_2 - d_{32}t_1 + 2c_{13}t_2 + d_{23}t_1 - 2c_{12} - d_{21} - 2c_{23}t_1 + d_{12} - d_{13}t_2 \\ d_{22}t_1 - d_{31} - d_{21}t_2 + d_{33}t_1 \\ -d_{12}t_1 + d_{11}t_2 + d_{33}t_2 - d_{32} \\ -d_{13}t_1 - d_{23}t_2 + d_{11} + d_{22} \\ -d_{31}t_2 + d_{32}t_1 + 2c_{13}t_2 - d_{23}t_1 - 2c_{12} + d_{21} - 2c_{23}t_1 + d_{12} - d_{13}t_2 \\ d_{13}t_1 - d_{23}t_2 - d_{11} + d_{22} \\ -d_{12}t_1 + d_{11}t_2 - d_{33}t_2 + d_{32} \\ -d_{31}t_2 + d_{32}t_1 + 2c_{13}t_2 + d_{23}t_1 - 2c_{12} - d_{21} - 2c_{23}t_1 - d_{12} + d_{13}t_2 \\ -d_{22}t_1 - d_{31} + d_{21}t_2 + d_{33}t_1 \\ d_{31}t_2 - d_{32}t_1 + 2c_{13}t_2 - d_{23}t_1 - 2c_{12} + d_{21} - 2c_{23}t_1 - d_{12} + d_{13}t_2 \end{bmatrix},$$

$$\mathbf{D}_{t_1} = \begin{bmatrix} c_{13}h_4 + c_{23}h_5 - d_{13}h_4 - 2c_{23}\lambda - d_{23}h_5 - d_{33}h_6 - c_{12}h_7 + c_{23}h_9 + d_{22}h_8 + d_{12}h_7 + d_{32}h_9 + d_{23}\lambda - d_{32}\lambda \\ -c_{23}h_8 + d_{22}\lambda + c_{23}h_6 + d_{33}\lambda \\ -c_{13}h_6 - d_{12}\lambda + c_{12}h_9 + c_{23}h_7 \\ -c_{23}h_4 + c_{13}h_5 - d_{13}\lambda - c_{12}h_8 \\ c_{13}h_4 - c_{23}h_5 - d_{13}h_4 - 2c_{23}\lambda - d_{23}h_5 - d_{33}h_6 - c_{12}h_7 - c_{23}h_9 + d_{22}h_8 + d_{12}h_7 + d_{32}h_9 - d_{23}\lambda + d_{32}\lambda \\ c_{23}h_4 + c_{13}h_5 + d_{13}\lambda - c_{12}h_8 \\ c_{13}h_6 - d_{12}\lambda - c_{12}h_9 + c_{23}h_7 \\ -c_{13}h_4 + c_{23}h_5 - d_{13}h_4 - 2c_{23}\lambda - d_{23}h_5 - d_{33}h_6 + c_{12}h_7 - c_{23}h_9 + d_{22}h_8 + d_{12}h_7 + d_{32}h_9 + d_{23}\lambda + d_{32}\lambda \\ c_{23}h_8 - d_{22}\lambda + c_{23}h_6 + d_{33}\lambda \\ -c_{13}h_4 - c_{23}h_5 - d_{13}h_4 - 2c_{23}\lambda - d_{23}h_5 - d_{33}h_6 + c_{12}h_7 + c_{23}h_9 + d_{22}h_8 + d_{12}h_7 + d_{32}h_9 - d_{23}\lambda - d_{32}\lambda \end{bmatrix},$$

$$\begin{aligned}
D_{t_2} &= \begin{bmatrix} -c_{13}h_1 + d_{33}h_3 + d_{23}h_2 + 2c_{13}\lambda - d_{11}h_7 - c_{13}h_9 - d_{21}h_8 + d_{13}h_1 - c_{12}h_8 - c_{23}h_2 - d_{31}h_9 - d_{13}\lambda + d_{31}\lambda \\ c_{13}h_8 - c_{23}h_3 - c_{12}h_9 - d_{21}\lambda \\ d_{33}\lambda + c_{13}h_3 + c_{11}\lambda - c_{13}h_7 \\ -c_{13}h_2 + c_{12}h_7 - d_{23}\lambda + c_{23}h_1 \\ -c_{13}h_1 + d_{33}h_3 + d_{23}h_2 + 2c_{13}\lambda - d_{11}h_7 + c_{13}h_9 - d_{21}h_8 + d_{13}h_1 + c_{12}h_8 + c_{23}h_2 - d_{31}h_9 - d_{13}\lambda - d_{31}\lambda \\ -c_{13}h_2 - c_{12}h_7 - d_{23}\lambda - c_{23}h_1 \\ -d_{33}\lambda - c_{13}h_3 + c_{11}\lambda - c_{13}h_7 \\ c_{13}h_1 + d_{33}h_3 + d_{23}h_2 + 2c_{13}\lambda - d_{11}h_7 + c_{13}h_9 - d_{21}h_8 + d_{13}h_1 - c_{12}h_8 - c_{23}h_2 - d_{31}h_9 + d_{13}\lambda - d_{31}\lambda \\ -c_{13}h_8 - c_{23}h_3 - c_{12}h_9 + d_{21}\lambda \\ c_{13}h_1 + d_{33}h_3 + d_{23}h_2 + 2c_{13}\lambda - d_{11}h_7 - c_{13}h_9 - d_{21}h_8 + d_{13}h_1 + c_{12}h_8 + c_{23}h_2 - d_{31}h_9 + d_{13}\lambda + d_{31}\lambda \end{bmatrix}, \\
D_{h_L} &= \begin{bmatrix} (d_{13} - c_{13})t_2 - d_{12} + c_{12} & (d_{23} - c_{23})t_2 - d_{22} & d_{33}t_2 - d_{32} - c_{23} & (c_{13} - d_{13})t_1 + d_{11} & (-d_{23} + c_{23})t_1 + d_{21} + c_{12} \\ 0 & c_{23} & -c_{23}t_2 & 0 & -c_{13} \\ -c_{23} & 0 & c_{13}t_2 - c_{12} & c_{13} & 0 \\ c_{23}t_2 & c_{12} - c_{13}t_2 & 0 & -c_{23}t_1 - c_{12} & c_{13}t_1 \\ (d_{13} - c_{13})t_2 - d_{12} + c_{12} & (d_{23} + c_{23})t_2 - d_{22} & d_{33}t_2 - d_{32} + c_{23} & (c_{13} - d_{13})t_1 + d_{11} & (-d_{23} - c_{23})t_1 + d_{21} - c_{12} \\ -c_{23}t_2 & c_{12} - c_{13}t_2 & 0 & c_{23}t_1 + c_{12} & c_{13}t_1 \\ -c_{23} & 0 & -c_{13}t_2 + c_{12} & c_{13} & 0 \\ (d_{13} + c_{13})t_2 - d_{12} - c_{12} & (d_{23} - c_{23})t_2 - d_{22} & d_{33}t_2 - d_{32} + c_{23} & (-c_{13} - d_{13})t_1 + d_{11} & (-d_{23} + c_{23})t_1 + d_{21} + c_{12} \\ 0 & -c_{23} & -c_{23}t_2 & 0 & c_{13} \\ (d_{13} + c_{13})t_2 - d_{12} - c_{12} & (d_{23} + c_{23})t_2 - d_{22} & d_{33}t_2 - d_{32} - c_{23} & (-c_{13} - d_{13})t_1 + d_{11} & (-d_{23} - c_{23})t_1 + d_{21} - c_{12} \end{bmatrix}, \\
D_{h_R} &= \begin{bmatrix} -d_{33}t_1 + d_{31} + c_{13} & d_{12}t_1 - d_{11}t_2 - c_{12}t_1 & d_{22}t_1 - d_{21}t_2 - c_{12}t_2 & (d_{32} + c_{23})t_1 - (d_{31} + c_{13})t_2 \\ c_{23}t_1 + c_{12} & 0 & -c_{23}t_1 + c_{13}t_2 & -c_{12}t_2 \\ -c_{13}t_1 & c_{23}t_1 - c_{13}t_2 & 0 & c_{12}t_1 \\ 0 & c_{12}t_2 & -c_{12}t_1 & 0 \\ -d_{33}t_1 + d_{31} - c_{13} & d_{12}t_1 - d_{11}t_2 - c_{12}t_1 & d_{22}t_1 - d_{21}t_2 + c_{12}t_2 & (d_{32} - c_{23})t_1 - (d_{31} - c_{13})t_2 \\ 0 & -c_{12}t_2 & -c_{12}t_1 & 0 \\ c_{13}t_1 & c_{23}t_1 - c_{13}t_2 & 0 & -c_{12}t_1 \\ -d_{33}t_1 + d_{31} - c_{13} & d_{12}t_1 - d_{11}t_2 + c_{12}t_1 & d_{22}t_1 - d_{21}t_2 - c_{12}t_2 & (d_{32} - c_{23})t_1 - (d_{31} - c_{13})t_2 \\ c_{23}t_1 + c_{12} & 0 & c_{23}t_1 - c_{13}t_2 & -c_{12}t_2 \\ -d_{33}t_1 + d_{31} + c_{13} & d_{12}t_1 - d_{11}t_2 + c_{12}t_1 & d_{22}t_1 - d_{21}t_2 + c_{12}t_2 & (d_{32} + c_{23})t_1 - (d_{31} + c_{13})t_2 \end{bmatrix}.
\end{aligned}$$

ACKNOWLEDGMENT

The work described in this paper was fully supported by a grant from the Research Grants Council of Hong Kong (project CityU117605).

REFERENCES

1. R. Valkenburg and A. McIvor, "Accurate 3D measurement using a structured light system," *Image Vis. Comput.* **16**, 99–110 (1998).
2. M. Wilczkowiak, P. Sturm, and E. Boyer, "Using geometric constraints through parallelepipeds for calibration and 3D modeling," *IEEE Trans. Pattern Anal. Mach. Intell.* **27**, 194–207 (2005).
3. Y. F. Li and S. Y. Chen, "Automatic recalibration of a structured light vision system," *IEEE Trans. Rob. Autom.* **19**, 259–268 (2003).
4. C. Huang, C. Chen, and P. Chung, "An improved algorithm for two-image camera self-calibration and Euclidean structure recovery using absolute quadric," *Pattern Recogn.* **37**, 1713–1722 (2004).
5. L. Quan and Z. Lan, "Linear N -point camera pose determination," *IEEE Trans. Pattern Anal. Mach. Intell.* **21**, 774–780 (1999).
6. X-S. Gao, and X.-R. Hou, J. Thang, and H.-F. Cheng, "Complete solution classification for the perspective-three-point problem," *IEEE Trans. Pattern Anal. Mach. Intell.* **25**, 930–943 (2003).
7. H. C. Longuet-Higgins, "A computer algorithm for reconstructing a scene from two projections," *Nature* **293**, 133–135 (1981).
8. A. Gruen and T. Huang, *Calibration and Orientation of Cameras in Computer Vision* (Springer-Verlag, 2001).
9. O. Faugeras and S. Maybank, "Motion from point matches: multiplicity of solutions," *Int. J. Comput. Vis.* **4**, 225–246 (1990).
10. R. Hartley, "Estimation of relative camera positions for uncalibrated cameras," in *Lecture Notes in Computer Science* (Springer-Verlag 1992), pp. 579–580.
11. B. Triggs, "Routines for relative pose of two calibrated

- cameras from 5 points," Tech. Rep. (INRIA, 2000) <http://www.inrialpes.fr/movi/people/Triggs>.
12. D. Nister, "An efficient solution to the five-point relative pose problem," *IEEE Trans. Pattern Anal. Mach. Intell.* **26**, 756–770 (2004).
 13. J. C. Hay, "Optical motion and space perception: an extension of Gibson's analysis," *Psychol. Rev.* **73**, 550–565 (1966).
 14. R. Tsai, T. Huang, and W. Zhu, "Estimating three dimensional motion parameters of a rigid planar patch, II: singular value decomposition," *IEEE Trans. Acoust., Speech, Signal Process.* **30**, 525–534 (1982).
 15. H. C. Longuet-Higgins, "The reconstruction of a plane surface from two perspective projections," *Proc. R. Soc. London, Ser. B* **227**, 399–410 (1986).
 16. Z. Zhang and A. Hanson, "Scaled Euclidean 3D reconstruction based on externally uncalibrated cameras," in *Proceedings of the International Symposium on Computer Vision* (IEEE, 1995), pp. 37–42.
 17. T. Ueshiba and F. Tomita, "Plane-based calibration algorithm for multi-camera systems via factorization of homography matrices," in *Proceedings of the Ninth IEEE International Conference on Computer Vision* (IEEE, 2003), Vol. 2, pp. 966–973.
 18. A. Raij and M. Pollefeys, "Auto-calibration of multi-projector display walls," in *Proceedings of the Ninth IEEE International Conference on Computer Vision and Pattern Recognition* (IEEE, 2004), Vol. 1, pp. 14–17.
 19. T. Okatani and K. Deguchi, "Autocalibration of a projector-camera system," *IEEE Trans. Pattern Anal. Mach. Intell.* **27**, 1845–1855 (2005).
 20. A. Habed and B. Boufama, "Camera self-calibration from bivariate polynomial equations and the coplanarity constraint," *Image Vis. Comput.* **24**, 498–514 (2006).
 21. G. Schweighofer and A. Pinz, "Robust pose estimation from a planar target," *IEEE Trans. Pattern Anal. Mach. Intell.* **28**, 2024–2030 (2006).
 22. R. Mester and M. Muhlich, "Improving motion and orientation estimation using an equilibrated total least squares approach," in *Proceedings of IEEE International Conference on Image Processing* (IEEE, 2001), Vol. 2, pp. 929–932.
 23. K. Kanatani and N. Ohta, "Accuracy bounds and optimal computation of homography for image mosaicing applications," in *Proceedings of IEEE, International Conference on Computer Vision* (IEEE, 1999), Vol. 1, pp. 73–78.
 24. P. Chen and D. Suter, "Homography estimation and heteroscedastic noise—a first order perturbation analysis," Tec. Rep. MECSE-32, (Monash University, 2005).
 25. A. Criminisi, I. Reid, and A. Zisserman, "A plane measuring device," *Image Vis. Comput.* **17**, 625–634 (1999).
 26. R. Hartley and A. Zisserman, *Multiple View Geometry in Computer Vision* (Cambridge U. Press, 2003), Chap. 5, pp. 132–150.
 27. B. Zhang, Y. F. Li and Y. H. Wu, "Self-recalibration of a structured light system via plane-based homography," *Pattern Recogn.* 1368–1377 (2007).
 28. R. Hartley, "Chirality," *Int. J. Comput. Vis.* **26**, 41–61 (1998).
 29. J. Weng, T. Huang, and N. Ahuja, "Motion and structure from two perspective views: algorithms, error analysis and error estimation," *IEEE Trans. Pattern Anal. Mach. Intell.* **11**, 451–476 (1989).
 30. C. Lu, D. Hager, and E. Mjolsness, "Fast and globally convergent pose estimation from video images," *IEEE Trans. Pattern Anal. Mach. Intell.* **22**, 610–622 (2000).
 31. P. M. Griffin, L. S. Narasimhan, and S. R. Yee, "Generation of uniquely encoded light patterns for range data acquisition," *Pattern Recogn.* **25**, 609–616 (1992).
 32. Z. Zhang, "A flexible new technique for camera calibration," *IEEE Trans. Pattern Anal. Mach. Intell.* **22**, 1330–1334 (2000).
 33. D. Fofi, J. Salvi, and E. Mouaddib, "Uncalibrated reconstruction: an adaptation to structured light vision," *Pattern Recogn.* **36**, 1631–1644 (2003).